Entropy Production in Finite-Difference Schemes

Ronald A. Cox* and Brian M. Argrow*
University of Oklahoma, Norman, Oklahoma 73019

Introduction

TO insure that shocks are accurately captured, the conservative form of the equations of motion of a fluid are typically solved. Since implicit numerical diffusion often prevents the formation of phenomena that violate the second law of thermodynamics, the second law is usually not solved. However, solutions computed with the high-accuracy total variation diminishing (TVD) schemes introduced in the early 1980s often violated the second law. In particular, expansion discontinuities often formed in first-order-accurate calculations of stationary wave fields. As a consequence, various modifications to the schemes were incorporated to insure that the correct solutions were obtained. Unfortunately, other forms of nonphysical entropy production can still occur. As a result, there has been an increase in interest in schemes that satisfy an entropy condition.[1-4]

To better quantify the source of numerical errors in finite difference schemes, we examine the level of entropy production associated with a variety of wave fields and schemes to determine the origin of nonphysical production. The concern is not solely that the scheme satisfies the second law but to what degree the second law is satisfied. To do this, the Riemann problem is investigated by solving the conservative form of the unsteady Euler equations. That is,

$$\frac{\partial \boldsymbol{Q}}{\partial t} + \frac{\partial \boldsymbol{E}}{\partial x} = 0 \tag{1}$$

where

$$\boldsymbol{Q} = (\rho,\ \rho u,\ E_t)^T$$

and

$$\boldsymbol{E} = [\rho u,\ \rho u^2 + p,\ (E_t + p)u]^T$$

The initial conditions consist of two quiescent states, designated L and R. For convenience, all variables are nondimensionalized with respect to conditions in the high-pressure side L.

Finite Difference Scheme

The governing equations are integrated in time using a discrete, conservation-law form of Eq. (1),

$$\boldsymbol{Q}_i^{n+1} = \boldsymbol{Q}_i^n - \frac{\Delta t}{\Delta x}(\boldsymbol{E}_{i+\frac{1}{2}}^n - \boldsymbol{E}_{i-\frac{1}{2}}^n) \tag{2}$$

The indices i and n refer to the spatial and temporal discretizations. The numerical flux $\boldsymbol{E}_{i+\frac{1}{2}}^n$ is an approximation to the true flux at the cell face. It is computed by a flux-difference splitting analysis based on Roe's approximate Riemann solver.[5] The numerical flux is represented as

$$\begin{aligned}\boldsymbol{E}_{i+\frac{1}{2}} &= \tfrac{1}{2}(\boldsymbol{E}_i + \boldsymbol{E}_{i+1} - \boldsymbol{D}_{i+\frac{1}{2}}\Delta \boldsymbol{Q}_{i+\frac{1}{2}}) \\ &+ \tfrac{1}{2}[(1-\omega)(\Delta \boldsymbol{E}_{i+\frac{1}{2}}^{+c} - \Delta \boldsymbol{E}_{i+\frac{1}{2}}^{-c}) \\ &+ (\omega)(\Delta \boldsymbol{E}_{i-\frac{1}{2}}^{+u} - \Delta \boldsymbol{E}_{i+3/2}^{-u})]\end{aligned} \tag{3}$$

where

$$\boldsymbol{D}_{i+\frac{1}{2}} = \boldsymbol{R}_{i+\frac{1}{2}}(\Lambda^+ - \Lambda^-)_{i+\frac{1}{2}}\boldsymbol{R}_{i+\frac{1}{2}}^{-1}$$

$$\Delta \boldsymbol{E}_{i+\frac{1}{2}}^{\pm c} = \boldsymbol{R}_{i+\frac{1}{2}}\hat{\Lambda}_{i+\frac{1}{2}}^{\pm}\Phi(\boldsymbol{\alpha}_{i+\frac{1}{2}},\ \beta_c \boldsymbol{\alpha}_{i+\frac{1}{2}\mp 1})$$

$$\Delta \boldsymbol{E}_{i+\frac{1}{2}\mp 1}^{\pm u} = \boldsymbol{R}_{i+\frac{1}{2}}\hat{\Lambda}_{i+\frac{1}{2}}^{\pm}\Phi(\boldsymbol{\alpha}_{i+\frac{1}{2}\mp 1},\ \beta_u \boldsymbol{\alpha}_{i+\frac{1}{2}})$$

$$\hat{\Lambda}^{\pm} = \Lambda^{\pm}\left(I - |\Lambda|\frac{\Delta t}{\Delta x}\right)$$

$$\boldsymbol{\alpha}_{i+\frac{1}{2}} = \boldsymbol{R}_{i+\frac{1}{2}}^{-1}\Delta \boldsymbol{Q}_{i+\frac{1}{2}}$$

$$\beta_u = 1 + 1/\omega$$

$$\beta_c = 1 + 1/(1-\omega)$$

For supersonic cases, a fix to the $u \pm a$ eigenvalues prevents the occurrence of a stationary expansion discontinuity at the sonic point, which violates the second law. For example,

$$\bar{\lambda} = \text{sign}(\lambda)\sqrt{\lambda^2 + (\epsilon a)^2}$$

where a is the speed of sound and ϵ is a free parameter, generally less than about 0.3.

This algorithm is a derivative of a scheme used by Chakravarthy and Osher.[6] It is at least second order accurate, and for the linear case it is stable for Courant numbers less than one. The term ω is a free parameter that allows a variety of schemes to be evaluated. More specifically, the cell-face flux is represented by a linear combination of a central ($\omega = 0$) and an upwind ($\omega = 1$) representation for $\boldsymbol{E}$. The minmod limiter is used to obtain high-accuracy TVD solutions:

$$\Phi(x,\ y) = \text{sign}(x)\ \max\{0,\ \min[|x|,\ \text{sign}(x)\ y]\}$$

Nonlimited and first-order-accurate solutions are obtained by setting $\Phi(x,\ y)$ equal to x and 0. Additional details can be found in Ref. 7.

Entropy Production

The amount of entropy in the domain consists of the entropy at time $t = 0$ together with any additional entropy produced by the numerical representation of the governing equations. This is calculated with

$$S^n = \sum_{i=1}^{N} \frac{p_i^n}{(\rho_i^n)^{\gamma-1}}\Delta x_i \tag{4}$$

The numerical production of entropy in the domain is computed with a simple two-point temporal difference of S. The jump in entropy across the shock wave is used to calculate the exact rate of production:

$$\dot{S} = \frac{\mathrm{d}}{\mathrm{d}t}S = \rho_R W[s] \tag{5}$$

The term $[s]$ is the jump in entropy across the shock and W is the shock speed.

Numerical results are presented for the initial conditions $p_L/p_R = 8$ and $\rho_L/\rho_R = 6$. For the sake of brevity, we focus on this single (subsonic) case. Results for other conditions were qualitatively similar. Unless stated to the contrary, the following values were used in all of the calculations: $\Delta t = 0.004$, $\Delta x = 0.01$, $t = 0.2$, $\omega = 0.6$, and $\epsilon = 0$. No entropy correction was applied since it should not be necessary for this subsonic case.

First-order-accurate, nonlimited second-order-accurate, and second-order-accurate TVD results are compared with the exact solution in Fig. 1. The variation of entropy in the domain is displayed in Fig. 2. For a sufficiently large time, the correct production rate develops, despite the lack of dissipa-

Received Jan. 14, 1992; revision received May 19, 1992; accepted for publication May 29, 1992.

*Assistant Professor, School of Aerospace and Mechanical Engineering. Member AIAA.

tive phenomena in the governing equations. However, an overproduction of entropy is associated with all three methods immediately after the integration is begun. As evident in the figure, the numerical production can swamp the real production in the domain. The level of overproduction is greatest for the first-order-accurate scheme and least for the nonlimited second-order-accurate scheme. The increase in entropy predicted by both the first-order and the TVD scheme is identical for the first step. For the jump initial conditions, the minmod limiter returns a value of zero for all evaluations, and hence first-order-accurate representations for the fluxes occur.

For a fixed spatial cell size, a reduction in time step had little effect on the excess production in the domain. A typical result is displayed in Fig. 2. If both Δt and Δx are reduced while a fixed ratio is maintained, the overproduction of entropy decreases linearly with grid spacing.

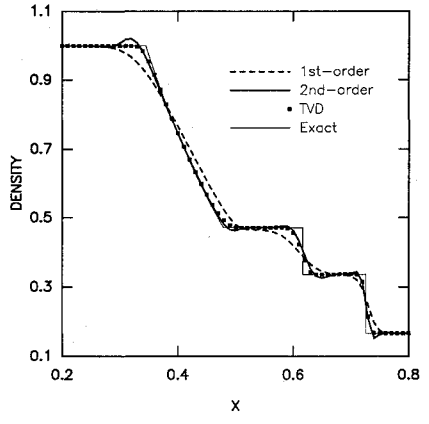

Fig. 1 Typical solutions of the Riemann problem ($p_L/p_R = 8$, $\rho_L/\rho_R = 6$, $t = 0.16$).

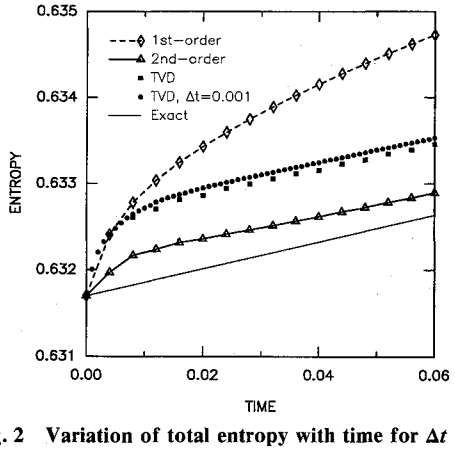

Fig. 2 Variation of total entropy with time for $\Delta t = 0.004$.

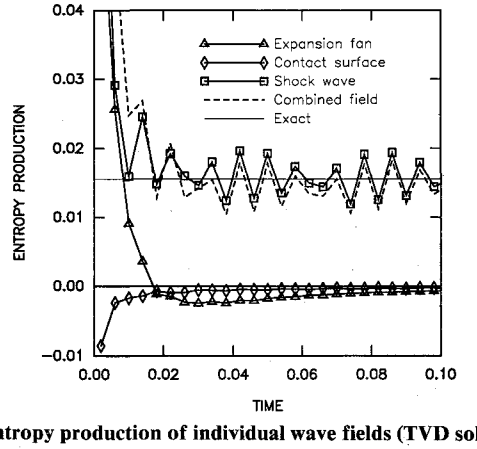

Fig. 3 Entropy production of individual wave fields (TVD solution).

To determine which wave field is responsible for the overproduction of entropy, the initial conditions are modified to correspond to each wave field separately. The flux of entropy into and out of the boundaries is accounted for in the calculation of $\dot{S}$ to isolate the production associated with the wave. The production associated with the three individual fields, together with the composite curve, is displayed in Fig. 3. There is a slight difference between the sum of the individual components and the composite field because of interactions between the fields in the startup phase of the calculations, before the discrete representations of the fields separate from each other.

During the startup process there is an overproduction of entropy associated with the expansion fan. This quickly drops (to a negative value) and asymptotes to the exact production rate (zero). The production in the expansion fan can be made positive by employing a large enough value for ϵ. This causes the expansion fan to diffuse to a greater extent and it increases the overproduction in the fan.

The entropy production associated with the contact surface is small and asymptotes to zero, but it is negative during the entire calculation. A variety of cases were examined, and this behavior was consistently observed.

The production associated with the shock is initially high, but it rapidly approaches the vicinity of the exact solution. The oscillations in the production are a result of the discrete representation of the shock wave. As grid points move through the shock, the entropy production varies. The importance of the discrete representation of the shock is discussed in Ref. 8.

For the composite TVD solution, the correct level of entropy production occurs when the three wave fields encompass a total of about five cells. For the test case examined here, this corresponds to a time of 0.02. In contrast, the production rate predicted by the first-order-accurate scheme does not approach the exact solution until $t = 0.3$. When an entropy peak occurs between the shock and the contact surface, limiting at the extrema may significantly slow the approach to the exact entropy-jump solution.

Acknowledgments

The authors gratefully acknowledge the many stimulating discussions with M. L. Rasmussen.

References

[1]Merriam, M. L., "An Entropy-Based Approach to Nonlinear Stability," NASA TM 101086, March 1989.

[2]Merriam, M. L., "Smoothing and the Second Law," *Computer Methods in Applied Mechanics and Engineering,* Vol. 64, No. 1, 1987, pp. 177–193.

[3]Tadmor, E., "The Numerical Viscosity of Entropy Stable Schemes for Systems of Conservation Laws. I," *Mathematics of Computation,* Vol. 49, No. 179, 1987, pp. 91–103.

[4]Schneider, G. E., and Kochavi, E., "A Control Volume Based Finite Element Formulation of the Compressible Flow Equations with Application to the Shock Tube Problem," AIAA Paper 89-1654, June 1989.

[5]Roe, P. L., "Approximate Riemann Solvers, Parameter Vectors, and Difference Schemes," *Journal of Computational Physics,* Vol. 43, No. 2, 1981, pp. 357–372.

[6]Chakravarthy, S. R., and Osher, S., "Computing with High-Resolution Upwind Schemes for Hyperbolic Equations," *Large-Scale Computations in Fluid Mechanics,* edited by B. E. Engquist, S. Osher, and R. C. J. Somerville, American Mathematical Society, Providence, RI, 1985, pp. 57–86.

[7]Cox, R. A., and Nishikawa, T., "A New Total Variation Diminishing Scheme for the Solution of Advective-Dominant Solute Transport," *Water Resources Research,* Vol. 27, No. 10, 1991, pp. 2645–2654.

[8]Roberts, T. W., "The Behaviour of Flux Difference Splitting Schemes Near Slowly Moving Shock Waves," *Numerical Methods for Fluid Dynamics III,* edited by K. W. Morton and M. J. Baines, Clarendon, Oxford, UK, 1988, pp. 442–448.